AVA and the effects of interference

SL1.7

*C.P.A. Wapenaar; * Taco S. van der Leij, and Aart-Jan van Wijngaarden, Delft University of Technology, The Netherlands*

Summary

Angle-dependent reflectivity sections are obscured by interference when the separation between the reflectors is less than half the seismic wavelength. These interference effects are angle-dependent and introduce a significant bias to AVA inversion schemes. In this paper we show that the *apparent* AVA effects related to the interference can be explained by the fact that for different illumination angles the medium is observed at different scales. We discuss several aspects of a true amplitude migration technique that corrects for apparent AVA effects, not only due to interference but also due to the dispersive effects related to the small scale variations of the medium parameters.

Introduction

Amplitude-versus-angle inversion (or AVA inversion) is generally based on Zoeppritz-like equations (non-linear or linearized) for *isolated* reflectors. However, when the layer thicknesses are in the order of -or smaller than- half the seismic wavelength, it is no longer justified to consider the reflectors as being isolated (Ostrander, 1984). The interference of the band-limited responses of the consecutive reflectors is angle-dependent. This introduces an *apparent* AVA behavior that may be quite different from the AVA behavior as predicted by the Zoeppritz equations for the individual reflectors. To illustrate this, we consider a horizontally layered acoustic constant velocity medium, with density variations only, see Figure 1. The motivation for this choice is given by the fact that the reflection coefficients of the individual reflectors are *angle-independent*, so any apparent AVA behavior will show up immediately. Figure *2* shows the primary reflection response of this medium in the *p*, T-domain. The rayparameter p is related to the propagation angle ϕ according to $p = (\sin\phi)/c$, where c is the propagation velocity. By converting the intercept time τ to depth z, according to $z = c\tau/2\cos\phi$, the angle-dependent reflectivity section *(p,* z-section) of Figure 3 is obtained. Figure *4* shows an amplitude cross section of Figure *3* at z = 556m. Note that this Figure exhibits apparent AVA behavior, despite the fact that the local reflection coefficient is angle-independent. Needless to say that a local inversion of this AVA curve would lead to erroneous medium (contrast-) parameters.

The main aim of this paper is to analyze apparent AVA due to angle-dependent interference and to propose a method for obtaining *p,* z-sections that are free of apparent AVA. The inversion of this type of sections (for elastic media) is discussed in a companion paper (van Wijngaarden and Wapenaar, 1995).

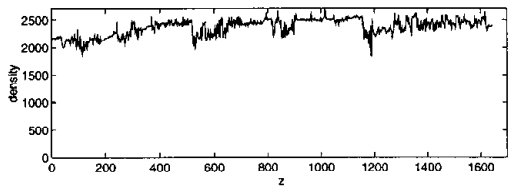

Figure 1: Density log (acoustic constant velocity medium)

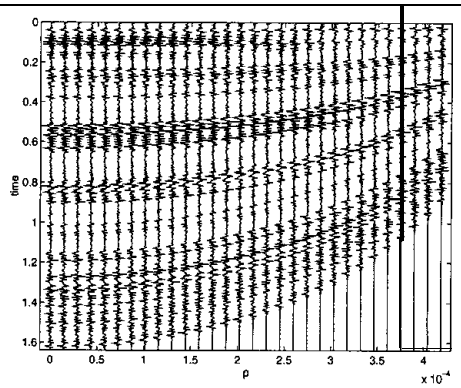

Figure 2: Primary reflection response

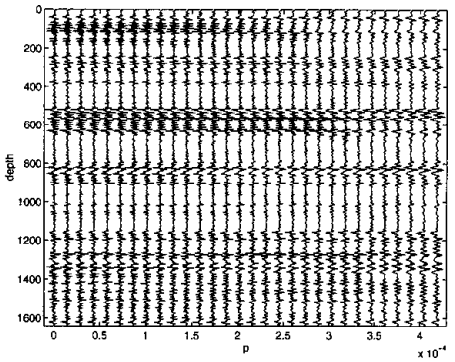

Figure 3: Angle-dependent reflectivity section with apparent AVA

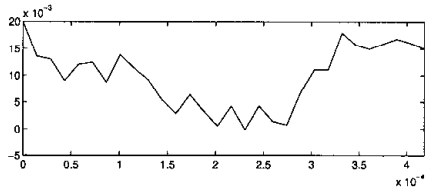

Figure 4: Amplitude cross section at z = 556m

Analysis of apparent AVA

The apparent AVA behavior observed in Figures 3 and *4* is easily explained with the aid of Figure *5.* This Figure shows two plane waves, illuminating the horizontally layered medium under two different angles. The frequency w has been chosen the same for both angles. As a result, the vertical wave length λ_z in the right frame is different from the wavelength λ in the left frame. In other words, for different illumination angles, the medium is observed at

different scales. This can be remidied by changing the frequency ω for different angles, such that the vertical wave length λ_z remains constant (Figure 6). For a constant velocity medium, λ_z and ω are related according to

$$\lambda_z = \frac{2\pi c}{\omega \cos\phi}, \quad \text{where} \quad \cos\phi = \sqrt{1 - c^2 p^2}. \tag{1}$$

Hence, in order to make λ_z independent of the propagation angle ϕ, the frequency ω should be chosen such that $\omega \cos \phi$ is constant. The upper frame in Figure 7 shows the p, ω−domain, where the shaded area denotes the seismic data and where the dashed lines are curves of constant λ_z. The shaded area in the lower frame in Figure 7 represents the pass-band of a filter, enclosed by two curves of constant λ_z. Note that this filter has a constant *spatial* bandwidth. We applied this "preconditioning filter" to the data of Figure 2 and we converted the result from time to depth, again according to $z = c\tau/2\cos\phi$. The result is shown in Figure 8. Note that the apparent AVA effects have been removed completely at the cost of some loss of resolution at the small propagation angles[1]. Obviously, any proper AVA inversion scheme applied to this section would yield an accurate (band-limited) reconstruction of the density log of Figure 1 (see van Wijngaarden and Wapenaar, 1995).

In the following sections we show how the ideas presented so far can be generalized for more realistic situations.

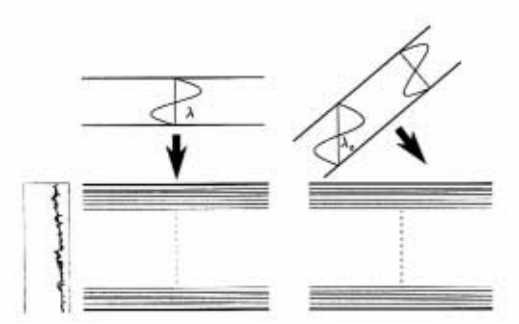

Figure 5: Different angles, same $\omega \Rightarrow \lambda_z \neq \lambda$

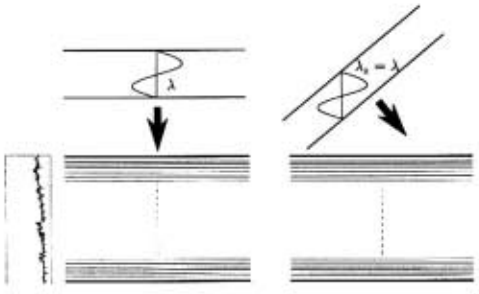

Figure 6: Different angles, different $\omega \Rightarrow \lambda_z = \lambda$

[1]For $p = 0$ the maximum frequency is reduced to $\omega_{max}\cos\phi_{max} = \omega_{max}\sqrt{1 - c^2 p_{max}^2}$, see Figure 7. Hence, for a maximum propagation angle of 30 degrees the resolution loss for vertical propagation is approximately 13 percent. Van Wijngaarden and Wapenaar (1995) discuss how to avoid this resolution loss altogether.

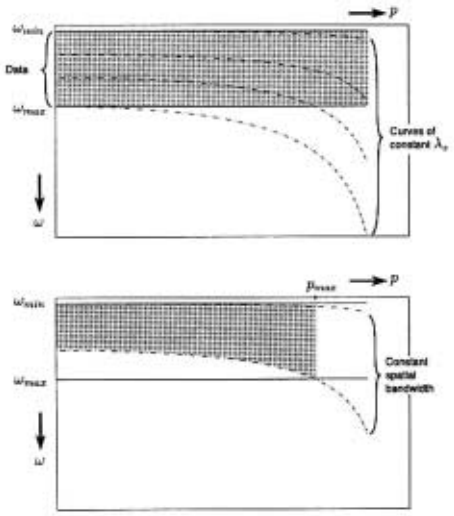

Figure 7: Upper frame: data with constant temporal bandwidth; Lower frame: preconditioning filter with constant spatial bandwidth

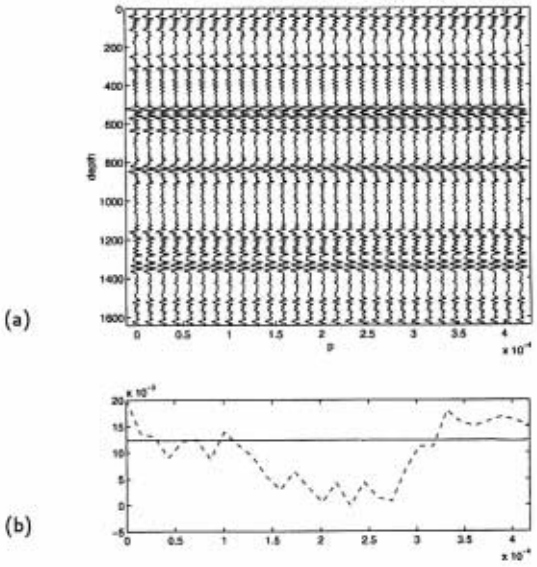

Figure 8: (a)Angle-dependent reflectivity section without apparent AVA. (b) Amplitude cross section at z = 556m (solid), compared with the previous result (dashed)

Angle-dependent reflectivity imaging

Another cause for apparent AVA is the anisotropic dispersion related to the small scale variations of the medium parameters (fine detail). At the 1994 SEG meeting we have presented a 3-D one-way representation of seismic data, that fully accounts for this effect. For the acoustic situation the representation for the upgoing wave field P^- has the following form

$$P^-(\mathbf{x}_D, \omega) = \int_\Omega W_g^-(\mathbf{x}_D, \mathbf{x}, \omega)\hat{R}^+(\mathbf{x}, \omega)W_g^+(\mathbf{x}, \mathbf{x}_S, \omega)S(\omega)d^3\mathbf{x}, \tag{2}$$

where the *generalized primary* propagators W_g^+ and W_g^- account for propagation, including the dispersion effects of the fine detail, and where the reflection operator $\hat{R}^+$ is a spatially filtered version of the true reflection operator. Finally, S(w) is the source function and Ω denotes the lower half-space. True amplitude migration aims at resolving the band-limited reflection operator $\hat{R}^+$ by inverting the generalized primary propagators W_g^+ and W_g^-, eliminating them from the data and applying an appropriate imaging principle. At the 1993 SEG meeting we have presented a method for inverting these propagators in a stable way, using power reciprocity to estimate the dispersion effects from the multi-dimensional cross-correlation of the reflection measurements. The resulting inverse propagators F_g^+ and R" compensate for the "propagation related" apparent AVA effects.

In the current paper we analyze the imaging principle, particularly paying attention to the "reflection related" apparent AVA effects that were discussed in the previous sections. For the sake of a simple discussion we consider a horizontally layered medium. We come back to this in the conclusions.

For a horizontally layered medium, equation (2) may be written in the rayparameter-frequency domain, according to

$$\tilde{P}^-(p,z_0,\omega) = \int_{z_0}^{\infty} \tilde{W}_g^-(p,z_0,z,\omega)\tilde{R}^+(p,z)\tilde{W}_g^+(p,z,z_0,\omega)S(\omega)dz. \tag{3}$$

For this situation, true amplitude migration involves *downward extrapolation,* according to

$$\tilde{P}^-(p,z,\omega) = \tilde{F}_g^-(p,z,z_0,\omega)\tilde{P}^-(p,z_0,\omega)\tilde{F}_g^+(p,z_0,z,\omega), \tag{4}$$

($\tilde{F}_g^{\pm}$ is the inverse of $\tilde{W}_g^{\pm}$), followed by *imaging,* according to

$$\langle\tilde{R}^+(p,z)\rangle = \frac{2\cos\bar{\phi}(p,z)}{\pi\bar{c}(z)}\Re\int_{\omega_1/\cos\bar{\phi}(p,z)}^{\omega_2(z)/\cos\phi(p,z)}\left(\frac{P^-(p,z,\omega)}{S(\omega)}\right)d\omega, \tag{5}$$

where $\Re$ denotes that the real part is taken, $\bar{c}(z)$ is the depth-dependent macro velocity and $\bar{\phi}(p,z)$ is the propagation angle in the macro model, according to $\cos\bar{\phi}(p,z) = \sqrt{1-\bar{c}^2(z)p^2}$. Inspired by the results of the previous sections (see in particular Figure 7), we have chosen a p-dependent integration interval, with $\omega_1 = \omega_{min}$ and ω_2 (x) being an appropriately chosen maximum frequency. The effect of the varying integration interval and of the scaling factor 2 cos $\bar{\phi}(p,z)/\pi\bar{c}(z)$ becomes clear when we analyze equations (3) through (5) for the situation of pre-critical primaries and a homogeneous macro model. We thus obtain from equation (3):

$$\tilde{P}^-(p,z_0,\omega) = \int_{z_0}^{\infty}\exp\left(\frac{2j\omega\cos\bar{\phi}}{\bar{c}}(z_0-z')\right)\tilde{R}^+(p,z')S(\omega)dz'; \tag{6}$$

from equations (4) and (6) :

$$\tilde{P}^-(p,z,w) = \int_{z_0}^{\infty}\exp\left(\frac{2jw\cos\bar{\phi}}{\bar{c}}(z-z')\right)\tilde{R}^+(p,z')S(\omega)dx'; \tag{7}$$

and from equations (5) and (7):

$$\langle\tilde{R}^+(p,z)\rangle = \frac{2\cos\bar{\phi}}{\pi\bar{c}}\int_{z_0}^{\infty}dz'\tilde{R}^+(p,z')\times \Re\int_{\omega_1/\cos\bar{\phi}}^{\omega_2/\cos\bar{\phi}}\exp\left(\frac{2jw\cos\bar{\phi}}{\bar{c}}(z-z')\right)dw, \tag{8}$$

or

$$\boxed{\langle\tilde{R}^+(p,x))} = \int_{z_0}^{\infty} b(z-z')\tilde{R}^+(p,z')dz', \tag{9}$$

where

$$b(x) = \frac{\sin(y) - \sin(y)}{\pi z}. \tag{10}$$

Apparently, the imaged reflectivity section $\langle\tilde{R}^+(p,z)\rangle$ is a spatially filtered version of the true reflectivity section $\tilde{R}^+(p,z)$. The filter b(z) describes the interference effects in the imaged section due to the finite bandwidth of the source function S(w). Note that b(z) is a bandpass filter, with *unit* amplitude in the passband $2\omega_1/\bar{c} < k_z < 2\omega_2/\bar{c}$. More importantly, note that this filter is *independent* of the rayparameter *p,* hence, the imaged section $\langle\tilde{R}^+(p,x)\rangle$ does not contain any apparent AVA effects! A result similar to equations (9) and (10) is obtained when we do a similar analysis for *generalized* primaries and an inhomogeneous macro model. In conclusion, we may state that equations (4) and (5) compensate, respectively, for the *propagation* and *reflection* related apparent AVA effects.

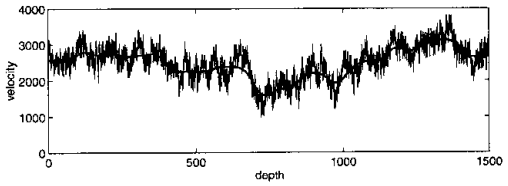

Figure 9: Velocity log (acoustic constant density medium; the heavy line represents the macro velocity $\bar{c}(z)$)

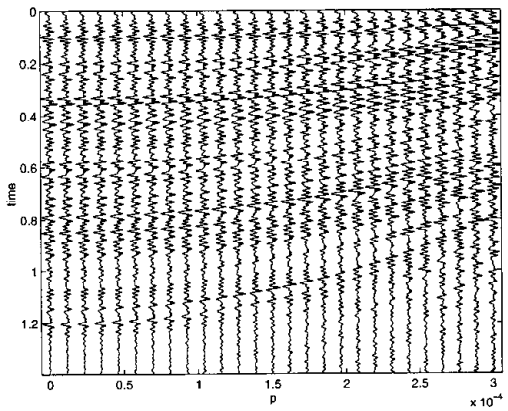

Figure 10: Exact reflection response

We illustrate the application of equations (4) and (5) with an example. Figure 9 shows a *velocity* log of an acoustic constant density medium. The transmission response of this log (i.e., the generalized primary propagator $\tilde{W}_g^{\pm}$) exhibits significant angle-dependent dispersion effects (not shown). We modeled the exact reflection response P^- (*p,* z_0, w), using a layer-code technique. The result in the *p,* T-domain is shown in Figure 10. We applied downward extrapolation and imaging, according to equations (4) and (5). The

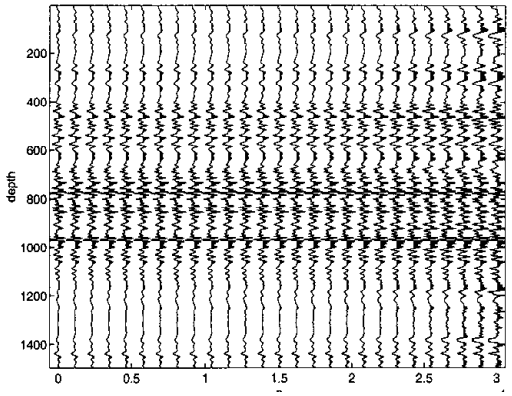

Figure 11: Imaged angle-dependent reflectivity section $\langle \tilde{R}^{+}(p,x) \rangle$

result, i.e. the imaged reflectivity section $\langle \tilde{R}^{+}(p,x) \rangle$, is shown in Figure 11. We zoomed in on the area around z = 980m. The result is shown in the upper frame of Figure 12. The middle frame in Figure 12 shows the same area, obtained after replacing $\tilde{F}_g^{\pm}$ in equation (4) by simple phase shift propagators. Hence, in this result the propagation related apparent AVA effects are ignored; only the reflection related AVA effects are taken into account. The lower frame in Figure 12 shows, for comparison, $\langle \tilde{R}^{+}(p,z) \rangle$ obtained directly from equation (9) where for $\tilde{R}^{+}(p,z')$ the true reflectivity section was taken and b(z - z') was designed for the macro velocity in the selected depth window. Figure 13 shows amplitude cross sections of the strongest positive wiggle in the vicinity of z = 980m. Note the excellent match up to $p = 3 * 10^{-4}\mathrm{s/m}$ (which corresponds to a propagation angle of 36 degrees) between the true amplitude migration result (solid) and the filtered true reflectivity section (dashed). Also note that the phase shift migration result (dotted) does not match the true result at all. Hence, this example shows that propagation related AVA effects may be just as important as the reflection related AVA effects.

Conclusions

We have shown that reflection related apparent AVA behavior in angle-dependent reflectivity sections can be explained by the fact that for different illumination angles the medium is observed at different scales (Figure 5). By applying an angle-dependent preconditioning filter (Figure 7) to the data, the spatial bandwidth (and thus the observed scale range) can be made constant for all angles, so that the apparent AVA effects vanish. This procedure works well for a horizontally layered medium with constant velocity and no significant dispersion effects related to fine-layering. For more general situations, the generalized primary representation (equation 2) should be inverted, thus accounting for propagation related as well as reflection related AVA effects. We have shown (both theoretically and with an example) how this can be done for a horizontally layered medium. In particular we showed that the w-integration interval in the imaging step (equation 5) should be made angle-dependent, similar as the preconditioning filter in Figure 7. The resulting angle-dependent reflectivity sections are free of apparent AVA and are the ideal input for AVA inversion schemes.

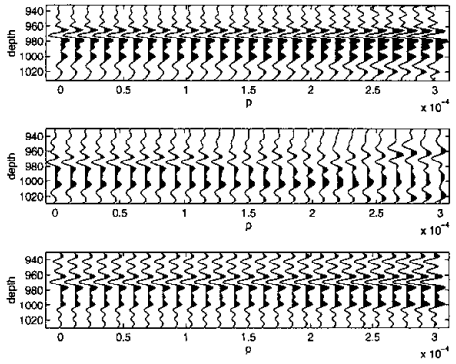

Figure 12: Selected area of Figure 1 1 (upper frame), compared with a result of phase shift migration (middle frame) and the filtered true reflectivity section (lower frame).

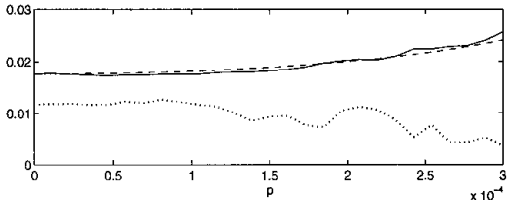

Figure 13: Amplitude cross sections of the positive wiggle at $z \approx$ 980m of the results of Figure 12 (solid, dotted, dashed, respectively)

The generalization for 2-D or 3-D inhomogeneous media is subject of current research. It involves a thorough study of the forward and inverse generalized primary propagators $W_g^{\pm}$ and $F_g^{\pm}$. Moreover, it involves a generalization of the proposed imaging principle, analogous to Vercruijsse et al. (1994) who apply a similar imaging principle (in the biangular domain) on isolated reflectors.

References

Herrmann, F.J., and Wapenaar, C.P.A., 1993, Wave propagation in finely layered media, a parametric approach: 63rd annual SEG meeting, Washington, 909-912

Ostrander, W.J., 1984, Plane-wave reflection coefficients for gas sands at nonnormal angles of incidence: Geophysics 49, 1637-1648

Vercruijsse, P.A., Fokkema, J.T., Peet, W.E., and De Roeck, G., 1994, Amplitude versus angle analysis of seismic data in the biangular domain : Submitted for publication in the Journal of Seismic Exploration

Wapenaar, C.P.A., and Herrmann, F.J., 1993, True amplitude migration taking fine layering into account: 63rd annual SEG meeting, Washington, 653-656

Wapenaar, C.P.A., 1994, Two-way and one-way representations of seismic data for highly heterogeneous media: 64th annual SEG meeting, Los Angeles, 1430-1433

van Wijngaarden, A. J., and Wapenaar, C.P.A., 1995, Resolution analysis in linearized elastic inversion: 65th annual SEG meeting, Houston